



This open access document is published as a preprint in the Beilstein Archives with doi: 10.3762/bxiv.2019.113.v1 and is considered to be an early communication for feedback before peer review. Before citing this document, please check if a final, peer-reviewed version has been published in the Beilstein Journal of Nanotechnology.

This document is not formatted, has not undergone copyediting or typesetting, and may contain errors, unsubstantiated scientific claims or preliminary data.

Preprint Title Antimony deposition onto Au (111) and insertion of Mg

Authors Zan Lingxing, Da Xing, Abdelaziz Abd-El-Latif and Helmut Baltruschat

Publication Date 01 Okt 2019

Article Type Full Research Paper

Supporting Information File 1 SUPPLEMENTARY INFORMATION.docx; 1.3 MB

ORCID® iDs Abdelaziz Abd-El-Latif - <https://orcid.org/0000-0002-4763-9827>

Antimony deposition onto Au (111) and insertion of Mg

Lingxing Zan^{a,b}, Da Xing^a, Abdelaziz Ali Abd-El-Latif^{a,c,d} and Helmut Baltruschat^{a,*}

^a Institut für Physikalische und Theoretische Chemie, Universität Bonn, Römerstraße 164,
D-53117 Bonn, Germany

^b Current address: Key Laboratory of Chemical reaction engineering of Shaanxi Province;
College of Chemistry & Chemical engineering, Yan'an University, Yan'an, 716000, P.R.
China

^c Current address: Accumulator Materials Research (ECM), Zentrum für Sonnenenergie- und
Wasserstoff-Forschung Baden-Württemberg (ZSW), Lise-Meitner-Str. 24, 89081 Ulm

^d Permanent address: National Research Centre, Physical Chemistry Dept., El-Bohouth St.
Dokki, 12311 Cairo, Egypt

*Corresponding author: baltruschat@uni-bonn.de

Antimony deposition onto Au (111) and insertion of Mg

Abstract

Magnesium based secondary batteries have been regarded as a viable alternative compared to the immensely popular Li-ion systems owing to its high volumetric capacity. One of the largest challenges is the selection of Mg anode material since the insertion/extraction processes are kinetically slow because the large ionic radius and high charge density of Mg^{2+} compared with Li^+ .

We prepared very thin films of Sb by electrodeposition on an Au (111) substrate. Monolayer and multilayer deposition (up to 20 Monolayer) were characterized by cyclic voltammetry and STM (Scanning-Tunneling-Microscope). Monolayer deposition results in a characteristic row structure; the monolayer is commensurate in one dimension, but not in the other. The row structure is to some extent maintained after deposition of further layers. After dissolution of the multilayers of Sb the substrate is roughened on the atomic scale due to alloy formation, as demonstrated by CV and STM. Further multilayer deposition correspondingly leads to rough deposit with protrusion of up to 3 nm.

The cyclic voltammogram for Mg insertion/de-insertion from $MgCl_2/AlCl_3$ /Tetraglyme (MACC/TG) electrolyte into/from Sb modified electrode shows a positive shift (400 mV) of the onset potential of Mg deposition compared to that at bare Au electrode. From the charge of Mg deposition, we find that the ratio of Mg to Sb is 1:1; and this somewhat less than expected for the Mg_3Sb_2 alloy.

Keywords: insertion/extraction, electrodeposition, alloy, STM, Au(111), antimony

Introduction:

Rechargeable batteries have become essential energy storing devices, which are widely used in portable electronic devices and hybrid electric vehicles. Magnesium based secondary batteries have been regarded as a viable 'environmental friendly, non-toxic' alternative compared to the Li-ion systems owing to its high volumetric capacity [1]. Unlike lithium, magnesium has no tendency to form dendrites during recharge [2] but on the other hand, Mg anode is covered with an insulation layer, differently from the formation of a solid electrolyte interface (SEI) layer, as known from Li. One of the main challenges in the commercialization of Mg-ion batteries is the incompatibility of magnesium anode with the electrolytes because the formation of this Mg^{2+} -film.

Recently, antimony (Sb) has been suggested as insertion material, because magnesium can form intermetallic with antimony. In addition, Sb has rhombohedral crystal structure, which can form alloy in a wide composition range [3, 4]. High initial capacity of 298 mAh/g at 1C rate has been reported for electrochemical magnesiumation at electrodeposited $Bi_{0.88}Sb_{0.12}$ alloy by Arthur et al. [4]. However, the capacity is declining to 215 mAh/g after 100 cycles with a mixture electrolyte of ethylmagnesium chloride, diethylaluminum chloride and anhydrous THF. A detailed, fundamental study of magnesium deposition/dissolution at Sb modified Au electrode surface has never been reported. Using this layer for such an insertion study in fundamental research offers the advantage of a better defined structure of the insertion compound than when using small particles as in battery research.

The initial study of antimony electrochemical deposition on Au electrode was done by cyclic voltammetry by Jung [5], who found that antimony deposition on Au(100) and Au(111) in acid electrolyte undergoes two electrochemical processes involving an irreversible adsorption and underpotential deposition. This irreversible adsorption was attributed to oxygenous Sb(III) species, probably SbO^+ , which is formed in acid electrolyte and is adsorbed irreversibly on Au surface at the potential more positive than the UPD potential [6]. Later, the fundamental research of this phenomenon of this irreversible adsorption and UPD of Sb was investigated by EC-STM. A detailed study on the structure of the irreversibly adsorbed oxygenous Sb(III) species and the Sb adlayer on Au(100) was carried out by Hara et al. and Yan et al. [6, 7]. Jung investigated the structure of the irreversibly adsorbed oxygenous Sb(III) species on Au(111) surface by an in situ STM [8] and Wu also [9] investigated the

electrodeposition of Sb on Au(111). It has been found that the formed adlayer has a $(\sqrt{3} \times \sqrt{3})R30^\circ$ structure on Au(111). The second process is the UPD process or the reduction of oxygenous Sb(III) species, which are from the bulk electrolyte. It was also investigated by other researchers [5, 9] [6, 7], but the structure of underpotentially deposited Sb adlayer on Au (111) was not resolved on an atomic level. It is well known that Sb [10] [11, 12], Bi [13-15], etc. can be used to form bimetallic semiconductors. These semiconductors possess has an interesting property and were widely used in the field of electrocatalysis and materials.

It is therefore the aim of the present study to examine the initial stages of Sb-deposition on Au (111). Furthermore, we demonstrate the insertion of Mg into multilayers of Sb on Au (111) using non-aqueous electrolyte (MACC in tetraglyme). The cycling reversibility of insertion/de-insertion will be studied. In an upcoming paper, we will study the kinetics of the insertion process in more detail. [25]

Experimental:

Chemicals, materials and electrolyte

The Au(111) single crystal was prepared by cooling down after flame annealing in pure argon (Air Liquid, 99.999 %,) atmosphere as described elsewhere [16]. A typical cyclic voltammogram of Au(111) in 0.1 M H₂SO₄ is shown in the inset of Fig. 1. The interpretation of the voltammetric feature of Au(111) has been reported before [17-19]. All aqueous electrolytes were prepared by 18.2 MΩ Milli-Q water and de-aerated with high purity argon gas for at least 15 min before use. Electrochemical measurements in 0.1 M H₂SO₄ (spectro pure grade) were implemented in a conventional three electrode glass-cell. 1 cm² Au sheet and RHE are used as a counter electrode and a reference electrode respectively. The electrochemical deposition of antimony at Au electrode was done in 0.25 mM Sb₂O₃ (99.999%, Aldrich) + 0.5 M H₂SO₄ electrolyte.

An Au(111) electrode and an antimony modified Au(111) electrode were used as working electrodes for Mg deposition measurements. Magnesium foil was used as a counter electrode and another one as a reference electrode. All the magnesium electrochemical deposition measurements were carried out in the MBraun glovebox (H₂O < 0.5 ppm, O₂ < 0.5 ppm). (In a similar manner as described in [25])

EC-STM measurements

All EC-STM measurements were performed with an Agilent Technologies 5500 Scanning Probe Microscope (SPM) and a commercially available STM scanner (Molecular Imaging/Agilent Technologies) fitted with an electrochemical cell so called STM/AFM cell as described before [20]. A Pt and Au wire was used as a quasi-reference electrode ($E_{\text{Pt/PtO}} = 0.9$ V vs. RHE) and a counter electrode, respectively. The reference electrode was immersed in a small compartment filled with the same electrolyte and separated from main compartment by a capillary. Pt/Ir (90:10) STM tips with a diameter of 0.25 μm were prepared by etching in a 2 M KOH + 4 M KSCN bath and coated with hot-melt glue containing different types of polymer (provided by Steinel) to minimize faradaic current. All the EC-STM measurements were done in glass chamber purged with argon at room temperature.

Preparation of MACC

All chemicals were purchased from Sigma-Aldrich. The Tetraglyme was distilled over sodium and stored over molecular sieves (3 Å) until the water content reaches to an amount less than 5 ppm. The water content has been determined by Coulometric Karl Fischer titration (Mettler Toledo). MgCl_2 was heated overnight under vacuum at 290°C and then stored under thionyl chloride for 1 week. At low pressure, the thionyl chloride was removed completely. All materials were handled in an Argon filled glovebox. The MACC electrolyte was prepared by adding tetraglyme (20.5ml) to MgCl_2 (0.966g). While stirring the AlCl_3 (1.368g) was added stepwise. The whole mixture was then stirred overnight after addition of an equivalent amount of MgH_2 to reduce the water content. (Analogous as described in [25])

Instruments:

All electrochemical measurements were carried out by a bi-potentiostat purchased from Pine Instruments Inc. model AFBPC1 in combination with LabVIEW software (National Instruments GmbH, Munich, Germany) for recording the cyclic voltammograms (CV).

Results and discussion

a) Electrochemistry of antimony on Au(111)

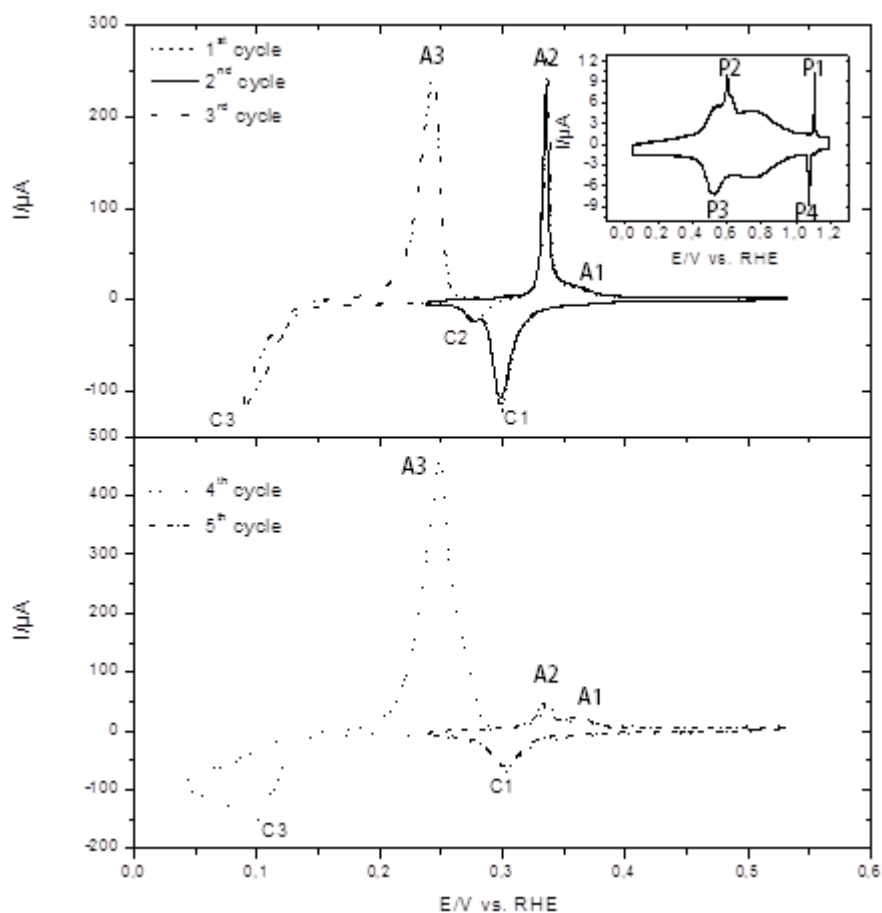


Fig. 1 Cyclic voltammograms of Sb deposition on Au(111) in 0.25 mM Sb_2O_3 + 0.5 M H_2SO_4 electrolyte saturated with Ar in H-cell at 10 mV s^{-1} . Inset: Cyclic voltammogram of Au(111) in 0.1 M H_2SO_4 solution saturated with Ar in H-cell at 50 mV s^{-1} to demonstrate the Au (111) surface.

The cyclic voltammograms of Sb underpotential deposition and overpotential deposition on Au(111) in 0.5 M H_2SO_4 containing 0.25 mM Sb_2O_3 electrolyte saturated by argon are shown in Fig. 1. Two peaks were observed in the underpotential deposition region. The first cathodic peak C1 ($\sim +0.3 \text{ V}$) is due to the reduction of preadsorbed oxygenous Sb(III) species (SbO^+). In a highly acidic electrolyte ($0 < \text{pH} < 1$), the main species of antimony is SbO^+ as reported by Wu et al. [9]. The following small peak C2 ($\sim +0.28 \text{ V}$) is due to the reduction of oxygenous Sb(III) species from bulk solution.

The total charge density of peaks C1 and C2 ($\sim 320 \mu\text{C cm}^{-2}$) suggests that the coverage of a monolayer is around 0.44 by assuming a one to one ratio of Sb to Au atoms for a hypothetical monolayer (and a $3 e^-$ process), which is close to the reported value of 0.43 [5]. However,

Itaya and coworkers [6] have investigated the Sb structure at Au(100) and they found the total charge due to Sb UPD and irreversible adsorption corresponding to the coverage of 0.63, which could be due to the influence of anions due to the co-adsorption. The charge of the corresponding dissolution peak A1 at +0.34 V amounts $290 \mu\text{C cm}^{-2}$. The charge ratio of the anodic peak A1 to the cathodic peaks C1 and C2 in the first potential cycle for Sb stripping/deposition in UPD region gives a value of 90 %. This residual 10% ($30 \mu\text{C/cm}^2$) may indicate some alloy formation from which Sb cannot again be deoxidised in the potential range and time scale of the experiment. Fig. 2 shows the cyclic voltammograms of Sb species/Au(111) electrodes which was induced by immersing the electrode surface into the Sb containing electrolyte for 1, 3 and 5 min at open circuit potential, in 0.1 M H_2SO_4 electrolyte. The electrode was rinsed with plenty of 0.1 M H_2SO_4 electrolyte before recording the CVs. The reduction and oxidation of Sb species on Au (111) were observed, suggesting that irreversible adsorption of Sb species, probably SbO^+ . On Au(111) starts the surface in contact with the Sb containing electrolyte at open circuit potential. These the cyclic voltammograms are similar and the charges of the cathodic peak in the first cycle in these three cases (contact for 1, 3 and 5min) are around $210 \mu\text{C cm}^{-2}$, indicating that the irreversible adsorption process is fast and the coverage of the irreversibly adsorbed Sb species on Au(111) is around 0.30 (assuming a $3e^-$ transfer), which is in good consistence with the value obtained in the literature [8]. It was also observed that the prolonged contact time ($\geq 1\text{min}$) did not effect on the CV on Au(100) electrode surface [6].

The reduction peak potential is identical to the first reduction peak C1 in fig.1. In agreement with literature, we can therefore conclude that peak C1 in fig.1 also corresponds to the reduction of the irreversibly adsorbed Sb species and peak C2 to further upd of Sb. The peak C1 observed by Wu [9] is smaller than that observed by us. We also observed a smaller peak C1 on polycrystalline Au electrode. Therefore, this difference is probably due to the roughness of the Au (111) surface, resulting from repeated alloying and dealloying during the cycling to obtain stable voltammetry in ref. Wu. Upon extension of the potential cycle to more negative potentials, bulk Sb starts around 0.13 V and gives rise to the peak C3 and the corresponding dissolution peak A3. Peak C1 and peak A2 largely decrease after extensive bulk deposition of nearly 2 monolayers in the fourth cycle. We attribute the decrease of peak A2 and C1 to the formation of a Au-Sb alloy in the bulk deposition region, An AuSb_2 surface alloy has been reported before by Stegemann [21] after deposition of Sb in UHV. Less Sb-UPD can form on Au-Sb alloy than on Au. In addition, less adsorbed Sb-species (SbO^+) is

adsorbed at positive potential, there the corresponding redox process becomes less convenient. The presence of anodic peak (A1) is then due to the stripping of Sb from the alloy. It is interesting to note that the difference between peaks C1+ C2 (now $146 \mu\text{C}/\text{cm}^2$) to that of A1+ A2 (now $100 \mu\text{C}/\text{cm}^2$) is with $40 \mu\text{C}/\text{cm}^2$ about the same as in the first cycle and probably corresponds to same continues incorporation of Sb into the surface to form the surface alloy.

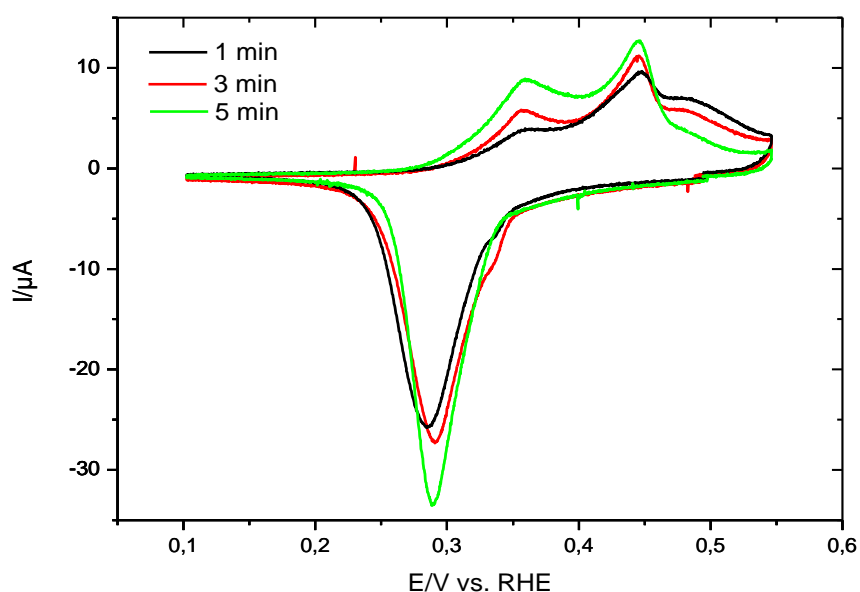


Fig. 2 Cyclic voltammograms of Sb species/Au(111) in 0.1 M H_2SO_4 electrolyte saturated with Ar at the sweep rate of 10 mV s^{-1} . The irreversible adsorption of Sb species on Au(111) was induced after the electrode surface contact with Sb containing electrolyte in the hanging meniscus configuration for 1, 3 and 5 min at open circuit potential ($\sim 0.6 \text{ V}$).

A nearly complete desorption of Sb from the Au (111) surface could only be achieved after extensive cycling in pure 0.1 M H_2SO_4 . Then, the sulfate adsorption peaks and the corresponding spike at 1.05 V becomes discernible (See fig. S1). Obviously, some Sb remains incorporated in the Au surface and the Au (111) surface does not recover complete smoothness.

The behaviour of Sb up on Au (111) is somewhat different from that on Pt (111). [22] There, after the first deposition of Sb in peak C1, (occurring at 0.4 V vs RHE), a roughening transition occurs and neither dissolution nor further deposition of Sb is occurring, whereas here in the case of Au (111), such an incorporation and decrease of the peak C1 occurs only after extension of the sweep to more negative potentials.

b) Electrochemical Scanning Tunneling Microscope (EC-STM) measurements on Sb/Au(111)

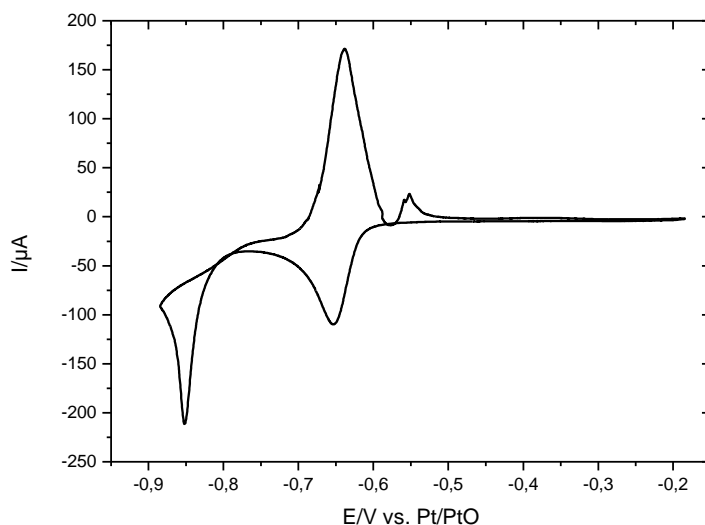


Fig. 3 Cyclic voltammogram of Sb deposition on Au(111) in 0.25 mM Sb_2O_3 + 0.5 M H_2SO_4 electrolyte in STM cell at 10 mV s^{-1} .

A similar cyclic voltammogram of Sb deposition on Au(111) in 0.25 mM Sb_2O_3 + 0.5 M H_2SO_4 electrolyte was obtained in STM cell during the STM measurements as shown in Fig. 3. It is similar to that recorded in the classical glass cell when the potential is converted to that versus reversible hydrogen electrode (RHE) using $E_{(\text{Pt}/\text{PtO})} \approx 0.9 \text{ V vs. RHE}$. The anodic monolayer oxidation peak is much smaller than the cathodic one, because of the extension of the sweep into the bulk deposition regions. However, the larger negative current flowing negative of the UPD peak and some superimposed negative current may be due to oxygen reduction, which starts at $\sim 0.36 \text{ V vs. RHE}$ (or $-0.54 \text{ V vs Pt/PtO}$) on Au electrode in 0.5 M H_2SO_4 [23]. The bulk deposition peak is much sharper because of the different diffusion behaviour in the small volume STM cell, which is somewhat resembling that of thin layer cells. (Bard, Faulstich) A further difference is that both anodic process are shifted in positive direction by 50 mV, which might be due to some instability of the pseudo reference electrode.

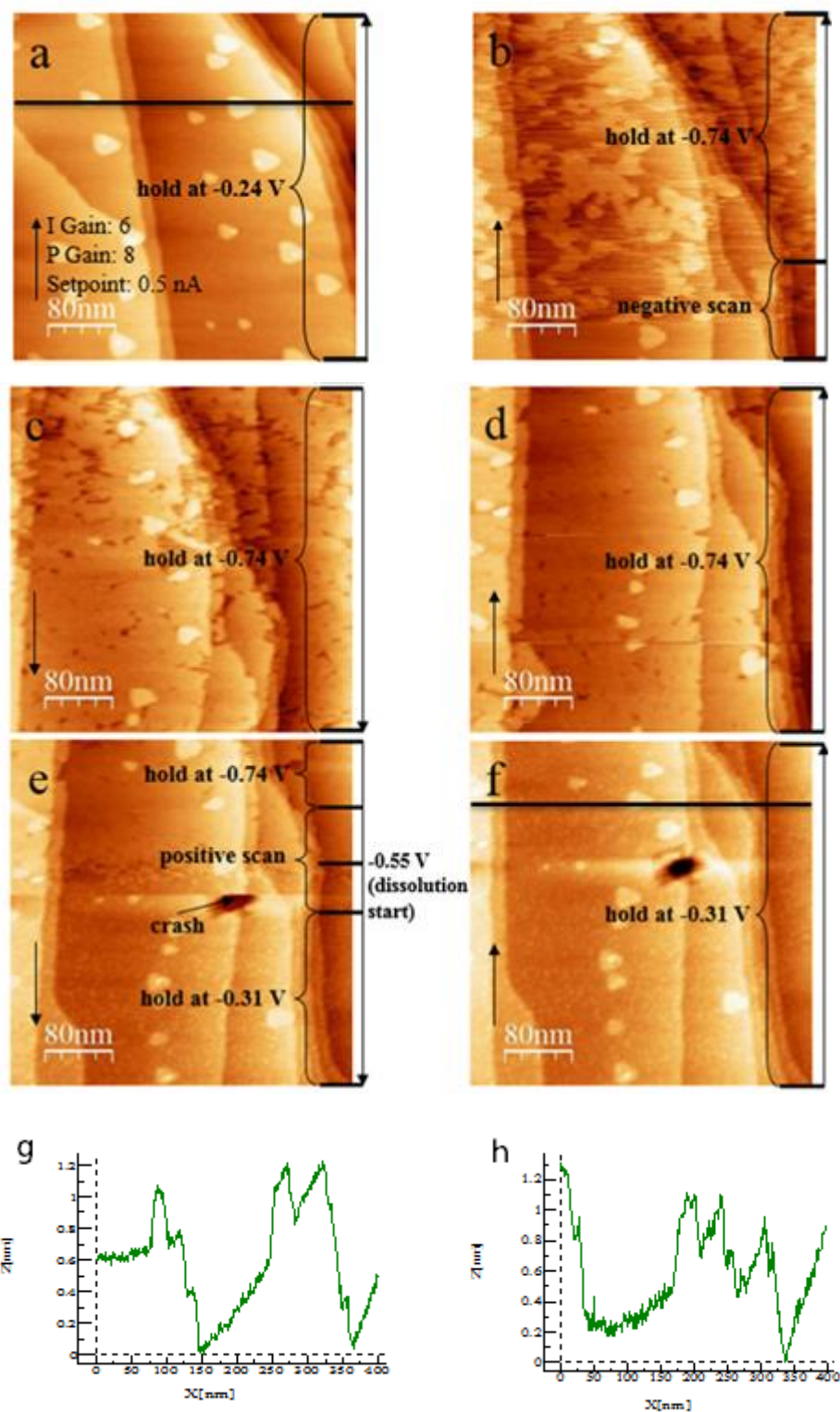


Fig. 4 Sequential STM topographic images of Sb deposition/dissolution on Au(111) in 0.25 mM Sb₂O₃ + 0.5 M H₂SO₄ electrolyte. (a) Initial Au(111) surface at open circuit potential of -0.24 V, (b) the electrode potential was scanned from -0.24 to -0.74 V and then stopped at -0.74 V, the height of Sb adlayer is shown with cross section in the image g, (c-d) the electrode potential was held at -0.74 V, formation of complete monolayer, (e) the electrode potential

was scanned back from -0.74 to -0.31 V and then stopped at -0.31 V, dissolution of monolayer (f) the electrode potential was held at -0.31 V. the two profiles below (g, h) are corresponding to the two black lines in image a and f. sample bias of 50 mV, set point = 0.5 nA & scan rate of 3.04 ln/s. Integral gain: 6 and proportional gain: 8. Arrows indicate scan direction. Line by line correction is used for above images.

An in situ observations of Sb underpotential deposition/dissolution on/from Au(111) surface in 0.5 M H₂SO₄ containing 0.25 mM Sb₂O₃ electrolyte in STM cell is shown in Fig. 4. In all EC-STM measurements, Pt/PtO electrode was used as reference electrode and the potential was scanned from -0.24 V (open circuit potential) to -0.74 V, which is in the potential range of UPD. At open circuit potential, the Au(111) surface is decorated by tiny particles and some small islands are observed as shown in Fig. 4a. These small Au islands are formed when the reconstruction of the Au(111) surface is lifted at the rest potential in solution. When the potential was scanned negatively, the nucleation on the terraces and epitaxial 2D growth started at ~-0.6 V (see. Fig. 4b). The Sb monolayer-islands were formed with the same height as the step height of the fresh prepared Au(111) which is 0.2 nm (see. Fig. 4a.). With the continuous growth at the potential of -0.74 V, a complete monolayer was formed within approximately 3.5 min as shown in Fig. 4c and d. However, this monolayer can be dissolved quickly when the potential was scanned positively to -0.31 V (see. Fig. 4e). But some tiny particles appeared on the surface after dissolution as shown in Fig. 4f, suggesting that the deposited Sb species cannot be dissolved completely and Au-Sb alloy was formed. This confirms the result obtained in electrochemical measurement.

The atomic resolution of Sb adlayer structure on Au(111) surface was obtained at the potential of -0.74 V and is shown in Fig. 5. As shown in Fig 5a, the distance between the rows is typically 2.4 to 3.2 nm. In different domains, their direction varies by 60°. However, in some cases also angles of approx. 20° were observed. The distance between two adjacent Sb atoms along the black dot line on image b is shown in Fig. 5d. To get accurate lattice parameters, the error induced by the thermal drift was eliminated by drift calibration and the Sb adlayer lattice vectors were corrected by using the calibration matrix from the known adlayer lattices of sulfate on Au(111), as outlined in detail by Iqbal, et al [20]. The orientation of the substrate was kept almost the same ($\pm 10^\circ$) for each experiment. The corrected distances between the two adjacent maxima invisible atoms along vector a and vector b (see. Fig. 5b) were found to be 1.076 nm and 0.821 nm, respectively. Both vectors include an angle of

114.6°, i.e. close to 120°. This spacing is considerably larger than that of the initial Sb adlayer which is formed by the reduction of the adsorbed oxygenous Sb species with the structure of $(\sqrt{3} \times \sqrt{3})R30^\circ$. From the area between the vectors a and b we estimate a packing density of the maxima of around 10 %, which is much less than that of the $(\sqrt{3} \times \sqrt{3})$ structure (theoretically 33%) and that calculated from the deposition charge (44 %) (Fig. 1). Roughly, only every fourth atom is visible on the STM picture, or every second in one dimension. Unfortunately, because of the incommensurability in the direction other than the row no structure model can be given.

The angle between the direction of the rows and the [110] direction of the substrate (that of the dense atomic rows) is very roughly 13°. Therefore we very tentatively assume for the vector in the direction of the rows $\vec{b} = (3,1) = \sqrt{13}R13.9^\circ$ with a theoretical length of $\sqrt{13} = 1.04 \text{ nm}$ involving one atom in an on top and another one in a bridge position (not visible), or, more likely, one atom in a three field hollow site position (not visible) and a further one in a near on top position (visible).

Wu also observed similar row structure of Sb on Au(111) [9], but it is not as clear as we observed. Similar row structure of Sb has been observed on Au(100) in perchloric acid electrolyte by Hara [6], who found that the irreversibly adsorbed SbO^+ adlayer has a quasi (2×2) structure and two adlayer structures, $(2\sqrt{2} \times \sqrt{5})$ and $(\sqrt{2} \times \sqrt{5})$ observed at 0.3 and 0.25 V, respectively.

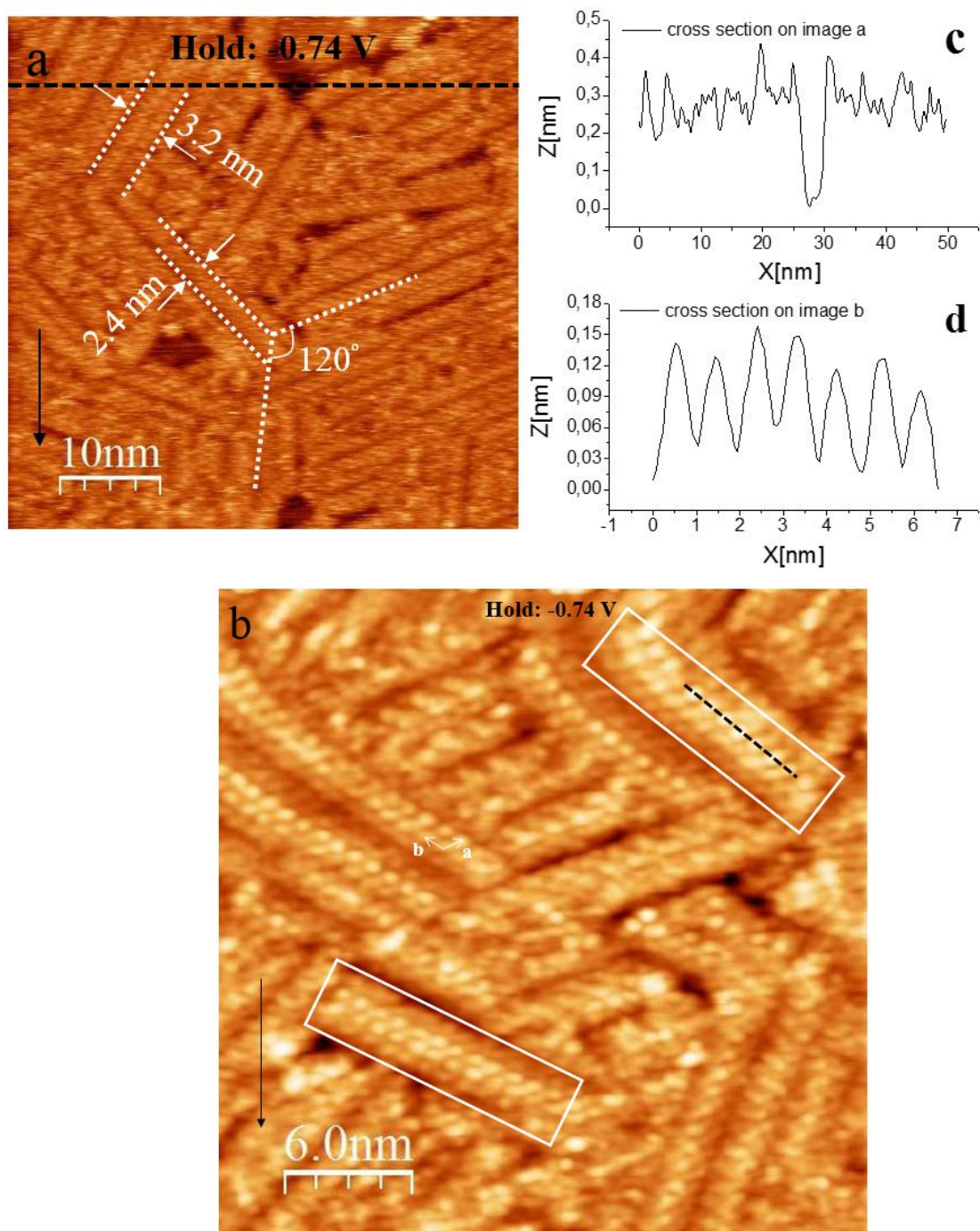
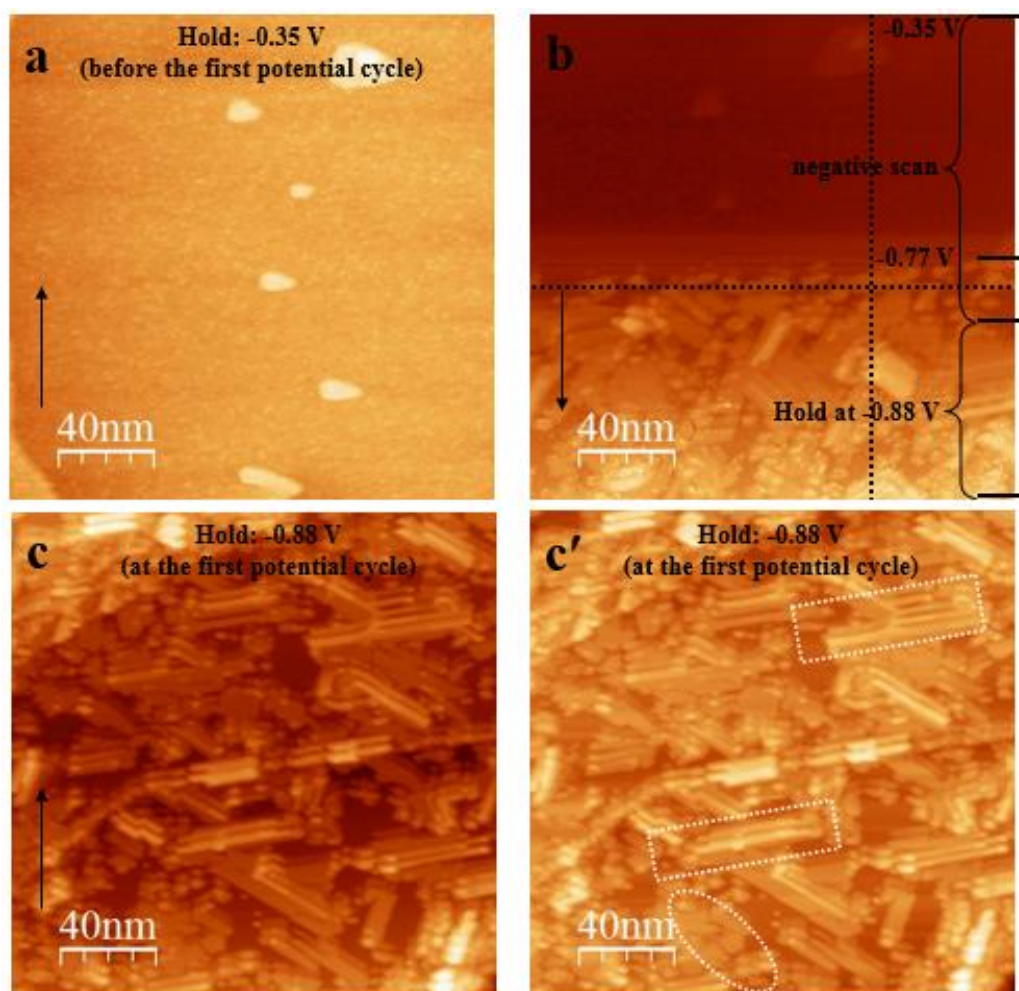


Fig. 5 STM images of the Sb adlayer structure on Au(111) in 0.25mM Sb_2O_3 + 0.5M H_2SO_4 electrolyte at -0.74 V. (a) 50×50 nm; (b) 30×30 nm; (c) the cross section on image a; (d) the cross section on image b. Sample bias of 50 mV, set point = 0.5 nA & scan rate of 12 ln/s. Integral gain: 2 and proportional gain: 3. Arrows indicate scan direction. Line by line correction is used for above images.

Bulk deposition of Sb on Au(111)

A freshly prepared Au(111) surface was employed for observing the bulk adlayer structure of Sb formed on its surface. The bulk deposition process is demonstrated in Fig. 6. The Au(111)

surface at the potential of -0.35 V in the Sb^{3+} containing electrolyte is shown in Fig. 6a. As the potential was scanned negatively from -0.35 to -0.88 V (see. Fig. 6b, c and c'), the bulk deposition of Sb starts at $\sim -0.8\text{ V}$ and both regular and irregular three dimensional (3D) structures are observed: row structures and island-like structures. The increase in the height of the Sb deposits with the initial decrease of the potential and then with the holding the potential at -0.88 V is shown in Fig. 6d. The horizontal cross section on Fig. 6b is shown in Fig. 6e. It shows that $\sim 1\text{ nm}$ height of Sb deposits was formed at that time. At the bottom of Fig. 6b, the height of the Sb deposits reaches to $\sim 6\text{ nm}$, which is around 30 layers. A somewhat atypical Stranski-Krastanov growth was thus observed during overpotential deposition.



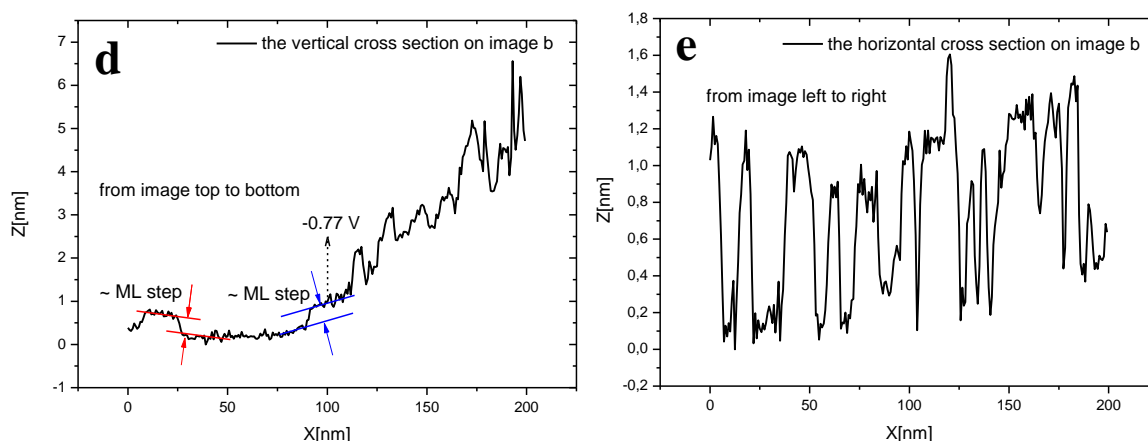


Fig. 6 STM images of Sb overpotential deposition on Au(111) during the first potential cycle in 0.25mM Sb_2O_3 + 0.5M H_2SO_4 electrolyte. (a) Initial Au(111) surface at the potential of -0.35 V, (b) the electrode potential was scanned negatively from -0.35 to -0.88 V and then stopped at -0.88 V, (c) and (c') the electrode potential was held at -0.88 V, (d) the cross section on the image b (black vertical dot line), (e) the cross section on the image b (black horizontal dot line). Sample bias of 50 mV, set point = 0.5 nA & scan rate of 3.04 ln/s. Integral gain: 6 and proportional gain: 8. Arrows indicate scan direction. Plane correction is used for images a, b and c. Line by line correction is used for image c'.

After stripping of Sb at -0.21 V the Au (111) substrate is not smooth again. Fig 7a shows the Au (111) surface after stripping of Sb at -0.21 demonstrating a severe roughness on the atomic scale. As shown in Fig 7 b) and c), the resulting Au (111) surface becomes more and more rough after each further deposition and dissolution process, which is an indication of the alloy formation [7, 21, 24]. The root mean square of the roughness (RMS roughness) of the terraces were determined to be 0.088, 0.095 and 0.130 on the image a, b and c, respectively. Subsequent deposition of Sb at -0.88 V during potential holds within following potential cycles are shown in Fig. 8. The deposited Sb with the row structure were also formed during the second potential cycle (see. Fig. 8a). However, most of the deposited Sb were turned to form a particle-like structure during the third and fourth potential cycle (see. Fig. 8b and c), but some of them with a row structure could still be found (see. Fig. 8d).

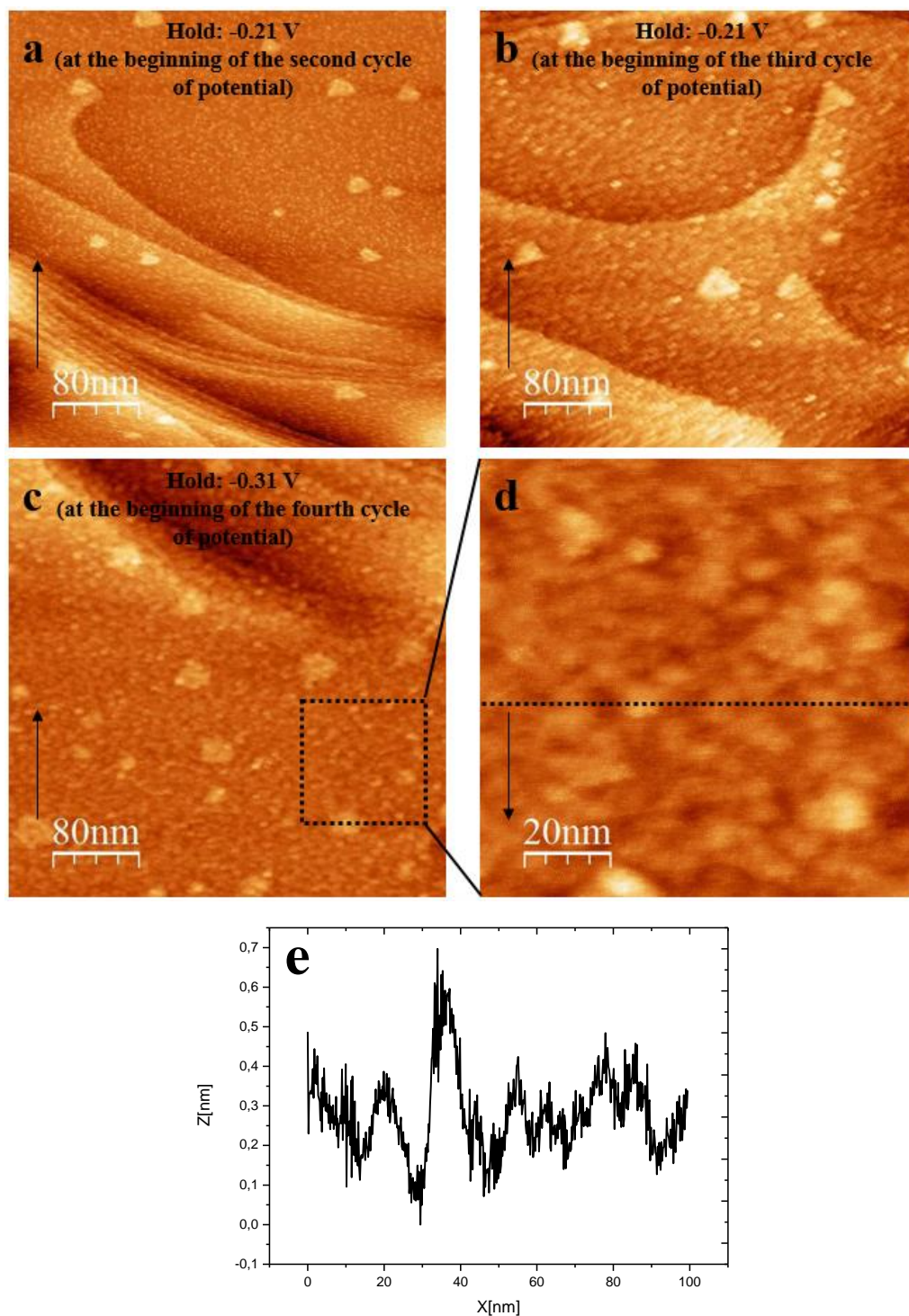


Fig. 7 STM images of Au(111) surface after Sb stripping in 0.25mM Sb_2O_3 + 0.5M H_2SO_4 electrolyte. (a) the potential was held at -0.21 V after the first potential cycle, (b) the potential was held at -0.21 V after the second potential cycle, (c) the potential was held at -0.31 V after the third potential cycle, (d) the zoomed in image on the image c (black box) and (e) the cross section on the image d (black dot line). Sample bias of 50 mV, set point = 0.5 nA & scan rate of 3.04 ln/s. Integral gain: 6 and proportional gain: 8. Arrows indicate scan direction. Line by line correction is used for above images.

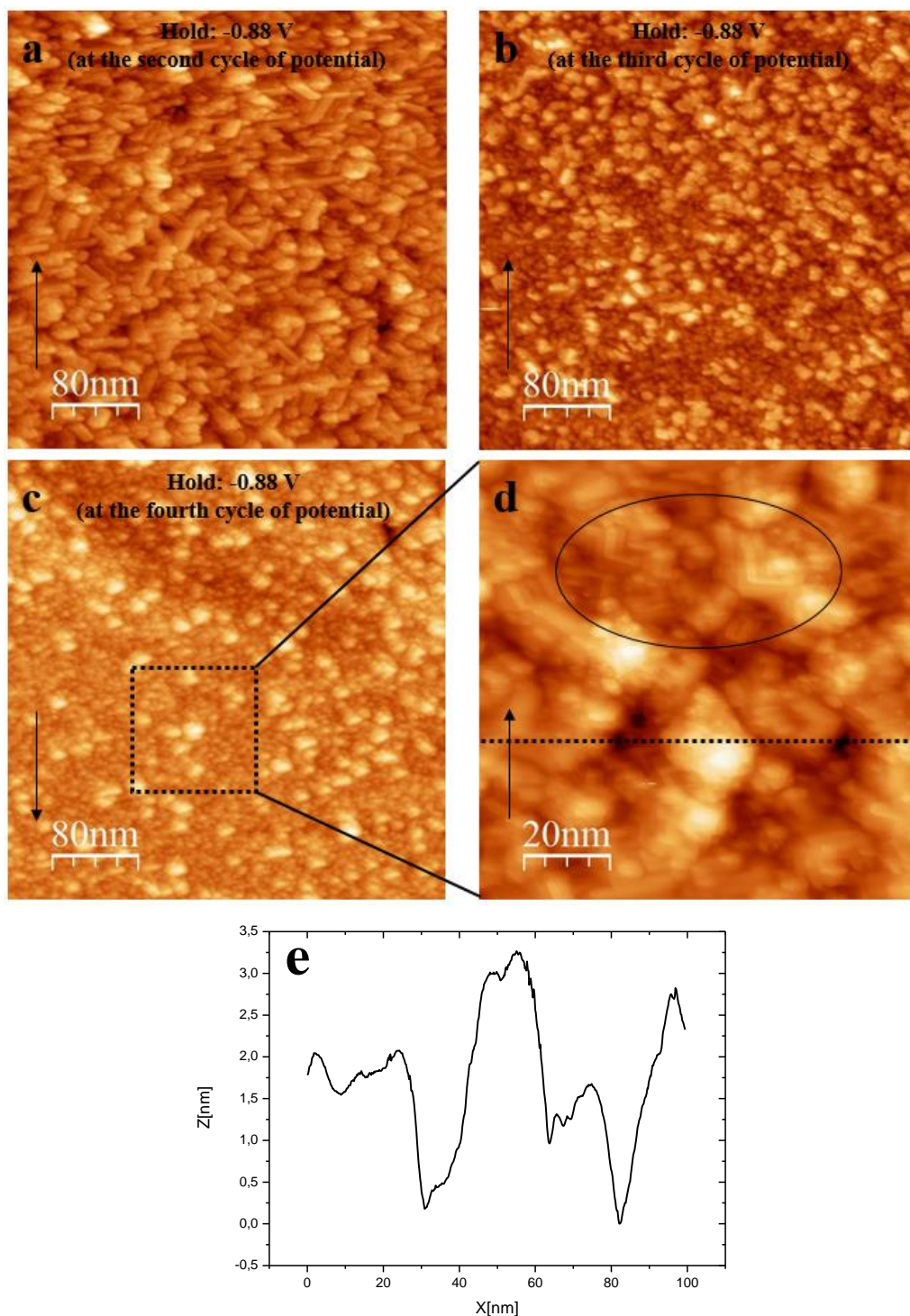
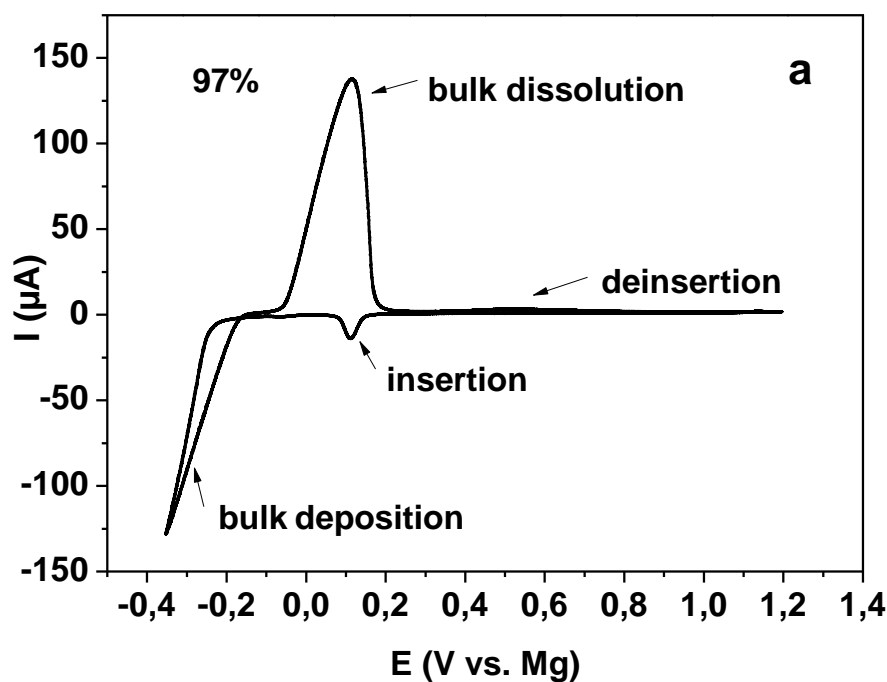


Fig. 8 STM images of Sb overpotential deposition on Au(111) in 0.25mM Sb_2O_3 + 0.5M H_2SO_4 electrolyte. (a) the potential was held at -0.88 V at the second potential cycle, (b) the potential was held at -0.88 V at the third potential cycle, (c) the potential was held at -0.88 V at the fourth potential cycle, (d) the zoomed in image on the image c (black box) and (e) the cross section on the image c (black dot line). Sample bias of 50 mV, set point = 0.5 nA & scan rate of 3.04 ln/s. Integral gain: 6 and proportional gain: 8. Arrows indicate scan direction. Line by line correction is used for above images.

Mg insertion and deposition

Fig. 9 shows the electrochemical deposition and stripping and insertion/de-insertion behavior of Mg into Sb-adlayer at Au(111) electrode in 0.5 M MgCl₂ + 0.5 M AlCl₃ in tetraglyme. The electrochemical deposition and stripping behavior of Mg at single crystalline gold electrode is similar to the behavior of Mg at a polycrystalline gold electrode. [25] The small peak at 0.1 V (vs. Mg) is due to the insertion of Mg into Sb-adlayer and not visible in the absence of Sb. Bulk deposition of Mg starts below -0.2 V. During the anodic going sweep, the current is still negative in the potential range of -0.35 to -0.2 V due to the continuous deposition of Mg. At E > (0.2 V), Mg is dissolved. The red curve in Fig. 9 is limited to the potential range positive of Mg bulk deposition. Therefore shows only the insertion/de-insertion behavior. The two observed peaks are the same as in the black curve, which indicates the insertion and de-insertion of Mg without Mg-bulk deposition. The ratio between the faradaic charge of anodic and cathodic gives the apparent coulombic efficiency. Therefore, 99.8% of the inserted magnesium is dissolved in the subsequent anodic sweep. The reversibility of the magnesium bulk deposition/dissolution is nearly 97%. From the Sb deposition charge (10.36 mC/cm²), the amount of the deposited Sb was calculated to be 20 monolayers, which is comparable to the STM results. The amount of the inserted Mg was 6.39 mC/cm². The ratio between the amounts of the inserted Mg (2e⁻) to the deposited Sb (3e⁻) was thus found to be 1:1, which is less than the theoretical value 3:2 (Mg₃Sb₂).



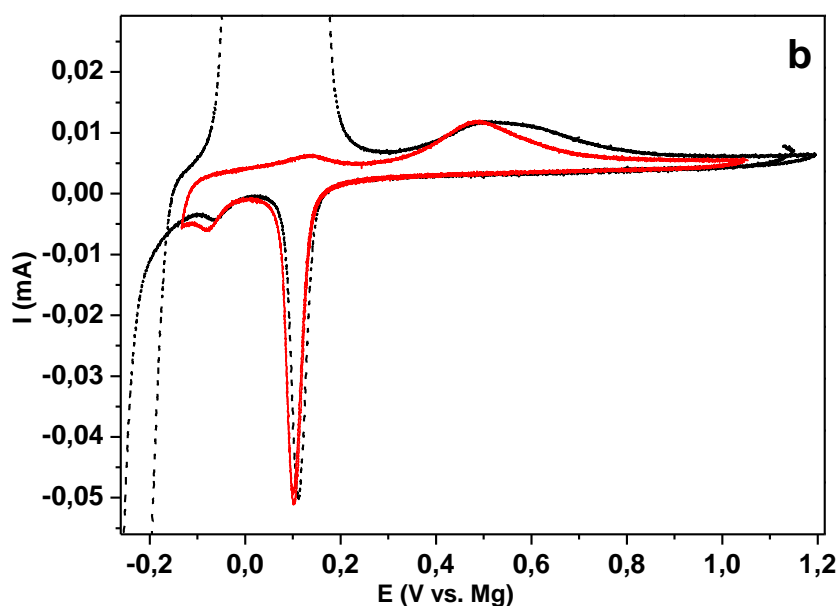
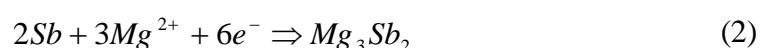


Fig. 9 a): Cyclic voltammograms of Mg deposition/dissolution and Mg insertion/deinsertion at single Au-electrode (Au 111) in MACC/tetraglyme at the sweep rate of 1 mV s^{-1} . b): Details of Mg insertion/de-insertion at Sb modified electrode in the potential range of -0.1 V to 1.1 V.

We attribute this to the insertion of Mg into the Sb-deposited layers and formation of magnesiated binary phase of antimony (Mg_3Sb_2), according to the following equation:



Where the onset potential is 400 mV more positive than that of bulk deposition at bare Au electrode (Fig. 9a and Fig S2). From the thermodynamic data for Mg_3Sb_2 alloy formation [26], $\Delta_f^\circ H = -300193.56 \text{ J/mol}$, and $\Delta_f^\circ S = -52.50 \text{ J/mol} \cdot \text{K}$, the calculated potential for Mg-Sb alloy formation at room temperature is $\sim 550 \text{ mV}$ (vs. Mg). Therefore, the experimental positive shift in the overpotential of Mg deposition during the insertion of Mg into Sb adlayers is in agreement with the theoretical value. After the saturation of the host-layers, bulk deposition of Mg started with the corresponding increase of the cathodic current. The discrepancy between the theoretical stoichiometry and the experimental deposition change ratios is explained by the thin Sb-layer, which does not allow a complete conversion to the bulk Mg_3Sb_2 -phase. In a forthcoming study, for somewhat thicker Sb layers on poly crystalline Au, we will show that the ratio of deposition charge for Mg and Sb is indeed 3:2.

[25] There, we will also give further evidence for the alloy formation and present a study on the rate of this process.

Conclusions

The electrochemical deposition of antimony on Au(111) was investigated in 0.5 M H₂SO₄ containing 0.25 mM Sb₂O₃ by cyclic voltammetry and electrochemical scanning tunneling microscopy (EC-STM). Two peaks were observed in the UPD region, one at 0.3 V due to the reduction of the irreversibly adsorbed oxygenous Sb(III) species and the other one at 0.28 V due to the reduction of oxygenous Sb(III) species from bulk electrolyte. The coverage of Sb monolayer was calculated to be 0.44 whereas the irreversible adsorption accounted for ~ 0.3. By observation with STM, Sb nucleation preferably starts at the active sites on the terrace, and then epitaxial 2D growth occurs to form the row structure with the width of ~2.4 or ~3.2 nm and the height of 0.35 nm. The angle between two different oriented domains is around 120°, which suggests that they are probably aligned along the densely packed (111) rows of the substrate. Some vacancies appeared between two parallel rows. The corrected distances between two Sb neighboring atoms were calculated to be 0.851 nm and 0.856 nm, respectively. The coverage of Sb UPD adlayer obtained from STM result is in a good agreement with the CV result. Furthermore, the bulk adlayer structure is depending on the roughness of the surface, which increased with the continuous deposition and dissolution of antimony in this case due to alloy formation between Sb and Au. Therefore, a structure change of the bulk adlayer from the row to particle-like structure was observed during the continuous potential cycles.

Magnesium deposition/dissolution on Au (111) with Sb modified electrodes was investigated in MACC. Interestingly, at the Sb modified Au electrode, a cathodic peak appears at 400 mV more positive than the onset potential of bulk deposition at Au electrode. We propose this potential shift is due to the formation of Mg₃Sb₂ alloy during the insertion of magnesium into Sb adlayers. High coulombic efficiencies of Mg stripping/insertion have been observed in cyclic voltammetry experiments.

Author contributions

L.X.Zan and A.A.Abd-El-Latif designed experiments and L.X.Zan, D.X and A.A.Abd-El-Latif performed electrochemical studies and characterization. L.X.Zan, D.X and A.A.Abd-El-Latif analysed, interpreted the data and wrote the manuscript.

Conflicts of interest

There are no conflicts of interest to declare.

Acknowledgments

A part of the results were presented as the Ph.D thesis by L.X Zan with the title “Metal-air Batteries: RRDE and EC-SPM Studies of Electrode Kinetics and Electrode Structure” (University of Bonn, Germany). The authors acknowledge funding by the Federal Ministry of Education and Research of Germany (BMBF, FKZ; 03EK3027A). L. Z. is grateful to the KAAD for a stipend.

References

- [1] J. Muldoon, C. B. Bucur, and T. Gregory, *Chemical Reviews* **114**:11683 (2014).
- [2] D. Aurbach, Y. Cohen, and M. Moshkovich, *Electrochemical and Solid-State Letters* **4**:A113 (2001).
- [3] Y. Cheng, Y. Shao, L. R. Parent, M. L. Sushko, G. Li, P. V. Sushko, N. D. Browning, C. Wang, and J. Liu, *Advanced Materials* **27**:6598 (2015).
- [4] T. S. Arthur, N. Singh, and M. Matsui, *Electrochemistry Communications* **16**:103 (2012).
- [5] G. Jung and C. K. Rhee, *Journal of Electroanalytical Chemistry* **436**:277 (1997).
- [6] M. Hara, J. Inukai, S. Yoshimoto, and K. Itaya, *Journal of Physical Chemistry B* **108**:17441 (2004).
- [7] J. W. Yan, Q. Wu, W. H. Shang, and B. W. Mao, *Electrochemistry Communications* **6**:843 (2004).
- [8] C. H. Jung and C. K. Rhee, *Journal of Electroanalytical Chemistry* **566**:1 (2004).
- [9] Q. Wu, W. H. Shang, J. W. Yan, and B. W. Mao, *Journal of Molecular Catalysis a-Chemical* **199**:49 (2003).
- [10] W. C. Butterman and J. J. F. Carlin, *Mineral Commodity Profiles: Antimony*, Unites States Geological Survey, 2003.
- [11] D. Xu, S. Shen, Y. Zhang, H. Gu, and Q. Wang, *Inorganic chemistry* **52**:12958 (2013).
- [12] H. Ipsier, H. Flandorfer, C. Luef, C. Schmetterer, and U. Saeed, *Journal of Materials Science: Materials in Electronics* **18**:3 (2007).
- [13] K. Jüttner, *Electrochimica Acta* **31**:917 (1986).
- [14] G. Kokkinidis, *Journal of Electroanalytical Chemistry and Interfacial Electrochemistry* **201**:217 (1986).
- [15] C. A. Jeffrey, D. A. Harrington, and S. Morin, *Surface Science* **512**:L367 (2002).
- [16] F. Hernandez, J. Sanabria-Chinchilla, M. P. Soriaga, and H. Baltruschat, in *Electrode Processes VII*, Vol. 18 (V.I. Birss, M. Josowicz, D. Evans, and M. Osawa, eds.), Electrochemical Society Proceedings, Pennington, 2004, p. 15.
- [17] H. Angerstein-Kozłowska, B. E. Conway, A. Hamelin, and L. Stoicoviciu, *Journal of Electroanalytical Chemistry* **228**:429 (1987).

- [18] S. Yasuda, R. Kumagai, K. Nakashima, and K. Murakoshi, *Journal of Physical Chemistry Letters* 6:3403 (2015).
- [19] E. Bunge, R. J. Nichols, B. Roelfs, H. Meyer, and H. Baumgartel, *Langmuir* 12:3060 (1996).
- [20] S. Iqbal, C. Bondul[^], and H. Baltruschat, *The Journal of Physical Chemistry C* 119:20515 (2015).
- [21] B. Stegemann, T. M. Bernhardt, B. Kaiser, and K. Rademann, *Surface Science* 511:153 (2002).
- [22] G. Jung, H. Park, and C. Rhee, *Journal of Electroanalytical Chemistry* 453:243 (1998).
- [23] R. Y. Wang, C. D. Wessells, R. A. Huggins, and Y. Cui, *Nano Letters* 13:5748 (2013).
- [24] A. R. Graham and S. Kaiman, *American Mineralogist* 37:461 (1952).
- [25] D.Xing,A.A.Abd-El-Latif, L.X. Zan, H. Baltruschat, Insertion / Extraction of Magnesium Ion into the Antimony Modified Au Electrode (In Progress).
- [26] A. A. Nayeb-Hashemi and J. B. Clark, *Bulletin of Alloy Phase Diagrams* 5 (1984).